Letter | Editors' Suggestion

Altermagnetism from interaction-driven itinerant magnetism

Samuele Giuli [1,*] Carlos Mejuto-Zaera [1] and Massimo Capone [1,2]
[1] *International School for Advanced Studies (SISSA), via Bonomea 265, 34136 Trieste, Italy*
[2] *CNR-IOM Democritos, Via Bonomea 265, 34136 Trieste, Italy*

(Received 6 October 2024; revised 11 December 2024; accepted 12 December 2024; published 3 January 2025)

Altermagnetism, a new phase of collinear spin-order sharing similarities with antiferromagnets and ferromagnets, has introduced a new guiding principle for spintronic and thermoelectric applications because of its direction-dependent magnetic properties. Fulfilling the promise to exploit altermagnetism for device design depends on identifying materials with tuneable transport properties. The search for intrinsic altermagnets has so far focused on the role of anisotropy in the crystallographic symmetries and in the band structure. Here, we present a different mechanism that approaches this goal by leveraging the interplay between a Hubbard local repulsion and the itinerant magnetism given by the presence of van Hove singularities. We show that altermagnetism is stable for a broad range of interactions and dopings and we focus on tunability of the spin-charge conversion ratio.

DOI: 10.1103/PhysRevB.111.L020401

Introduction. The landscape of magnetic systems has been thrilled by the proposal and experimental realization of altermagnetism, a new type of collinear spin-order, which shares similarities with both antiferromagnets and ferromagnets [1,2], while featuring new properties that hold a huge potential for fundamental science and applications. Altermagnets are characterized by a zero net magnetization in the nonrelativistic limit, similarly to antiferromagnets, but their electronic bands do not form a Kramer doublet, having instead a momentum-dependent spin splitting. Importantly, the magnetic polarization of an altermagnet has a long-range order with d-wave (or higher, g- or i-wave) symmetry characterized by nodes. The applicative potential of altermagnets relies mostly on the anisotropic magnetic properties, which have been proposed to give rise to giant magnetoresistance (GMR) [1], giant tunnel magnetoresistance [3], nonvanishing spin splitting torque [4,5] as well as anomalous Hall conductivity [6,7].

Despite the impressive and rapidly increasing body of work introducing candidate materials for altermagnetic ordering [8–25], there are still few experimental evidences of this phase of matter. This is in part owing to the lack of spin-resolved measurements and the small nonrelativistic spin splitting, which poses a challenge to its experimental resolution. For RuO_2 films various altermagnetic phases have been realized [26] while the debate for bulk RuO_2 [27,28] is still open. Other materials are under scrutiny as KV_2Se_2O [29] and $Rb_{1-\delta}V_2Te_2O$ [30]. Compelling evidence for altermagnetic ordering has been presented instead for MnTe [31] and CrSb [32].

Recently, it has been proposed that this direction-dependent magnetic phase could also arise from anisotropic local orbital states [33] where interactions can trigger the presence of an altermagnetic phase with the simultaneous realization of orbital and magnetic ordering.

In the search for intrinsic altermagnetic materials, most proposals have leveraged chemical and structural manipulation to tailor the electronic structure. Yet, recently an alternative approach to let altermagnetism arise from interactions has gained traction [10,20,33–37] but it has been addressed almost exclusively at mean-field level without accounting for strong correlation effects. This direction offers a particularly attractive perspective: devising platforms with *tunable* altermagnetic properties exploiting strong electronic correlations, which characterizes materials with narrow bands and comparatively large values of the screened Coulomb repulsion.

Indeed, the two traditional collinear magnetic phases, ferromagnetism and antiferromagnetism, are linked to strong correlation physics. Antiferromagnetism is an ubiquitous signature of strong correlations in undoped materials, while itinerant ferromagnetism is naturally connected with doped correlated materials.

The presence of ferromagnetism in the Hubbard model has been one of the driving forces behind the very introduction of the model. According to Nagaoka's theorem, it is the ground state for a single hole and large interactions [38], and it has been found in finite interactions [39–42] and for frustrated systems [43,44] as well. In the triangular lattice Hubbard model the presence of a van Hove singularity (vHs) at filling $n = 3/4$ appears to be fundamental for the formation of itinerant ferromagnetism [45] and also in the $t - t'$ square lattice Hubbard model [40,46]. In twisted bilayer graphene, the presence of a vHs near half-filling has also been linked to s-wave and $s\pm$-wave Pomeranchuk instabilities [47,48].

In this paper, building on the above arguments, we propose a paradigm where electronic correlations lead to the onset of altermagnetic ordering. Our proposal is based on a two-orbital model with anisotropic orbitals, and a van Hove singularity at moderate doping (see Fig. 1). We show that the altermagnetic

*Contact author: sgiuli@sissa.it

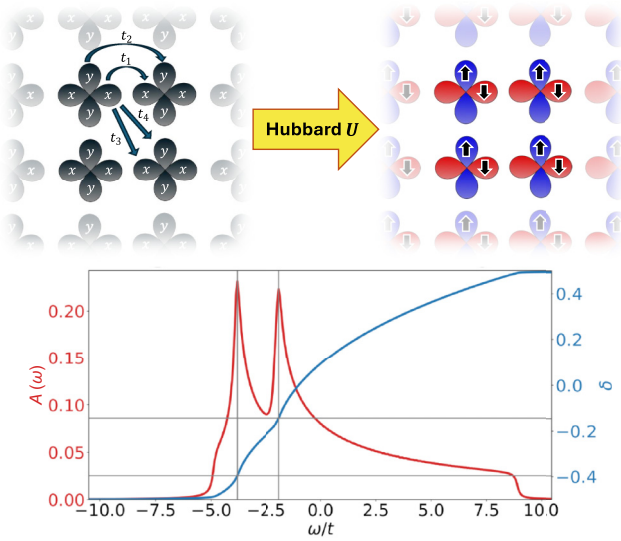

FIG. 1. Illustration of the interaction-driven phase transition from paramagnetic (top left) to altermagnetic (top right) and density of state of the noninteracting model (bottom-left axis) with doping (bottom-right axis) of the van Hove singularities in the noninteracting limit.

ordering naturally emerges with a uniform, on-site, nonrelativistic spin splitting as a result of the cooperation between the correlation-driven itinerant magnetism, the C_{4z} symmetry of inequivalent orbitals and a Hubbard-driven local spin exchange. Moreover, we show that the effect of interaction is not simply that of breaking the symmetry toward the altermagnetic phase but also renormalizing the bands and moving spectral weight from the quasiparticle peak to the Hubbard bands resulting in a drastic change in transport properties. This mechanism relies on intrinsic correlation effects owing to a local Hubbard repulsion that is not devised to explicitly break the spin and orbital symmetries. For this reason it can be realized in generic lattices even when spatial ordering is frustrated. These features are indeed quite generic and could inspire the *ab initio* and experimental search for altermagnetism candidates in unexplored classes of materials. We note that indeed the combination of the interaction-driven itinerant magnetism and the local exchange is necessary to stabilize the altermagnetic phase. It is in this sense that our proposed mechanism is truly driven by strong correlation, or in other words the competition between two different energy scales.

Model. We focus on a model introduced soon after the discovery of superconductivity in iron-based materials [41] as a minimal theoretical description. This model features two degenerate orbitals of d_{xz} and d_{yz} symmetry on each lattice site and local interactions parameterized by the intraorbital Hubbard U. The one-body Hamiltonian on a square lattice reads

$$\hat{H}_0 = \sum_{\mathbf{k},s} \begin{pmatrix} c^\dagger_{\mathbf{k}xs} & c^\dagger_{\mathbf{k}ys} \end{pmatrix} \begin{pmatrix} \epsilon_x(\mathbf{k}) & \epsilon_{xy}(\mathbf{k}) \\ \epsilon_{xy}(\mathbf{k}) & \epsilon_y(\mathbf{k}) \end{pmatrix} \begin{pmatrix} c_{\mathbf{k}xs} \\ c_{\mathbf{k}ys} \end{pmatrix} \tag{1}$$

with

$$\begin{aligned} \epsilon_x(\mathbf{k}) &= -2t_1 \cos k_x - 2t_2 \cos k_y - 4t_3 \cos k_x \cos k_y, \\ \epsilon_y(\mathbf{k}) &= -2t_2 \cos k_x - 2t_1 \cos k_y - 4t_3 \cos k_x \cos k_y, \\ \epsilon_{xy}(\mathbf{k}) &= -4t_4 \sin k_x \sin k_y. \end{aligned} \tag{2}$$

We set $t_1 = -t$, $t_2 = -1.75t$, $t_3 = -0.85t$, and $t_4 = -0.65t$, following Ref. [33]. This choice of parameters results in two van Hove singularities (vHs) in the bare density of states at doping $\delta_{vH} \approx -0.145$ and $\delta_{vH,2} \approx -0.396$. The existence of these vHs, together with the structure of the hoppings reflecting the d_{xz} and d_{yz} character of the orbitals, turn out to be the key ingredient to drive the altermagnetic state. Therefore, our results do not rely in the specific values of parameters as long as a vHs at reasonably small doping is present.

We will indeed focus on the doping region around the first vHs since the effect of the interaction around the second singularity is strongly reduced by the extreme doping. We introduce a purely intra-orbital Hubbard interaction, which, as discussed above, favors a ferromagnetic state close to a vHs on the single band Hubbard model [38–40]. The local interaction Hamiltonian therefore reads

$$\hat{H}_{\text{int}} = U \sum_{i,\alpha=x,y} \left(n_{i\alpha\uparrow} - \frac{1}{2} \right) \left(n_{i\alpha\downarrow} - \frac{1}{2} \right), \tag{3}$$

where $n_{i\alpha s}$ is the density operator at site i, orbital α, and spin s.

Method. We solve this model using the ghost rotationally invariant slave boson (gRISB) approach with mean-field boson decoupling [49], which is a generalization of RISB [50,51] and equivalent to the ghost Gutzwiller method [52]. This is a nonperturbative, variational Ansatz to capture strong electronic correlation in model as well as *ab initio* calculations of solids and molecules [49,52–60]. Within its embedding formulation, gRISB represents an interacting systems in terms of a pair of quasiparticle (qp) and impurity Hamiltonians. The latter captures local correlations exactly, while the former features interaction-renormalized hoppings and one-body potentials. The parameters of these Hamiltonians are determined self-consistently by matching their local one-body density matrices $\langle c^\dagger_\alpha c_\beta \rangle$, which makes the method computationally inexpensive [59,61,62]. Thus, we can use gRISB to rapidly and thoroughly explore the phase diagram of the multi-orbital model in Eqs. (1)–(3), obtaining faithful local order parameters from the impurity Hamiltonians, as well as nonlocal correlation functions from the band structure of the qp Hamiltonian. The description of correlated behavior in terms of a band structure theory greatly simplifies the study of the altermagnetic phase and its properties, and is enabled by the introduction of auxiliary states in the qp Hamiltonian, the eponymous ghosts. These ghosts enable capturing incoherent high-energy spectral features, for instance Hubbard bands, on top of the low-energy quasiparticle excitations [52,55,59]. Throughout the paper we fix the number of ghost orbitals per physical band to be $N_{\text{ghosts}} = 2$. The main equations of the gRISB formalism are summarized in the Supplemental Material (SM) [63].

Results. We define the local altermagnetic order parameter as

$$\Delta_{\text{alm}} = \frac{m_x - m_y}{2} \tag{4}$$

with $m_\alpha = n_{\alpha\uparrow} - n_{\alpha\downarrow}$ the spin magnetization on orbital $\alpha = x, y$. We present the ground-state phase diagram in Fig. 2. The presence of the vHs at doping $\delta_{vH} \approx -0.145$ (shown as a vertical, dashed line in Fig. 2) is linked to the onset

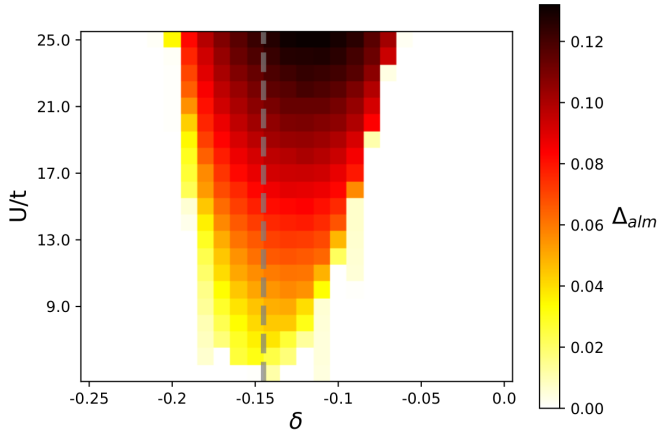

FIG. 2. Altermagnetic order parameter Δ_{alm} in Eq. (4) as a function of the interaction U and doping δ. The gray-dashed-vertical line indicates the doping of the van Hove singularity in the noninteracting model.

of spin ordering at large interaction U with two orbitals having opposite magnetization, realising the altermagnetic phase we propose in this paper. In contrast to previously proposed interaction-driven altermagnetic phases [33], we note that the opposite magnetic moments related by C_{4z} symmetry reside on *the same atomic site*. The altermagnetic ordering is enhanced and it extends to a larger range of dopings with increasing U/t while the maximum of the order parameter at fixed interaction is always found near $\delta = \delta_{vH}$. Significant interactions result therefore in a large doping region where altermagnetism is stable and sizable, avoiding the need for fine tuning the chemical potential, a particularly important point in view of applications to materials. The altermagnetic phase is also characterized by the momentum-dependent Zeeman splitting shown in the gRISB band structure on the right side of Fig. 3(a).

Our proposed altermagnetic state is energetically favorable with respect to a fully ferromagnetic one owing to the presence of interorbital hoppings that, together with the local repulsion U, favor antialignment of the spins between the orbitals (see the SM [63]). In addition, the presence of large next-nearest-neighbor hoppings [t_3 and t_4 in Eq. (2)] frustrates bipartite ordering, therefore we expect the altermagnet to be stable with respect to other uniform or nonuniform orderings. Further including interorbital interaction terms, that we neglected for the sake of simplicity, are not expected to destroy the altermagnetism as long the intraorbital U remains the largest energy scale, a condition, which holds under very general circumstances.

As we mentioned above, transport properties are amongst the most appealing features of altermagnets. For instance, these phases allow for spin-splitter effect when applying an electric field in the [110] direction. Since $\hat{S}_z$ remains a good quantum number, we can compute the spin-independent conductivity for spin-up and spin-down,

$$\sigma^s_{ab}(\omega) = -e^2 \frac{\left\langle \frac{1}{V_{BZ}} \sum_{\mathbf{k}} \partial_{k_a} \partial_{k_b} H^s_{\mathbf{k}} \right\rangle - \Lambda^s_{ab}(\omega)}{i(\omega + i0^+)} \tag{5}$$

with $s = \uparrow, \downarrow$, where $\Lambda^s_{ab}(\omega)$ is the s-spin current-current dynamical response that we compute as the elementary bubble without vertex corrections [64,65].

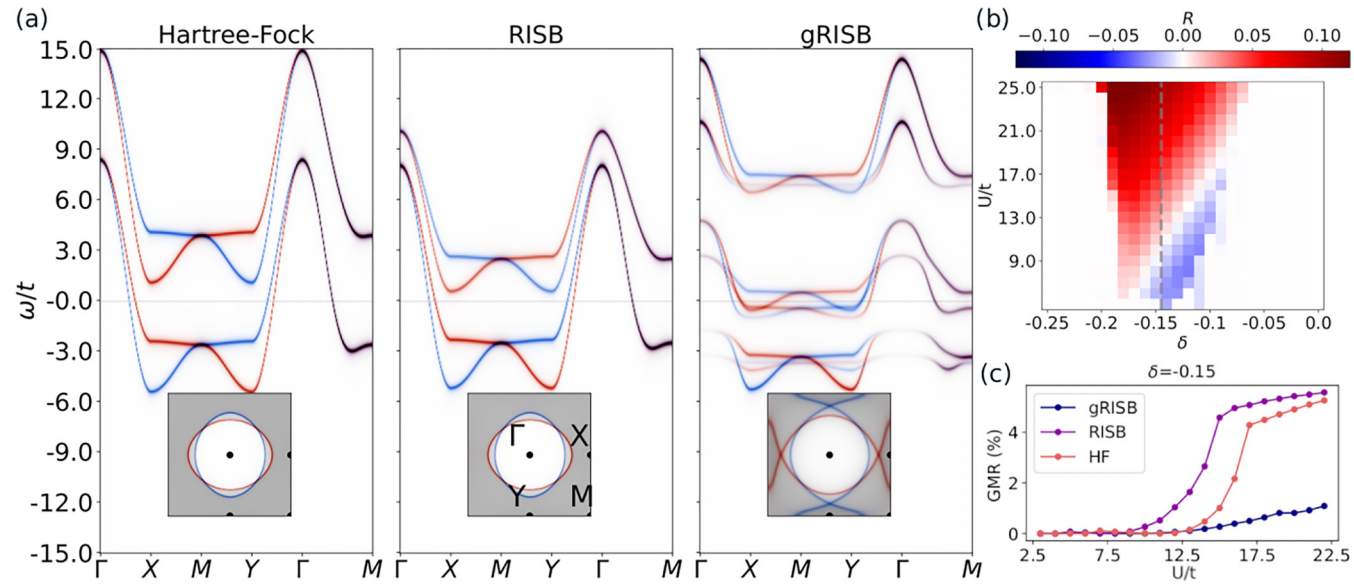

FIG. 3. (a) Spin-up (red) and spin-down (blue) spectral functions along symmetry lines for $U/t = 20$ and $\delta = -0.15$ using Hartree-Fock (left), RISB (center), and gRISB (right) with two ghosts. In the insets, the respective Fermi surfaces along the Brillouin zone, the shadowed area represent fermionic occupation: dark occupied, light empty. (b) Charge spin conversion ratio in Eq. (7) as a function of interaction (U/t) and doping (δ). Positive values correspond to spin-current in the $[-110]$ direction while a negative ones are in the opposite direction. The gray-dashed-vertical line indicates the doping of the van Hove singularity in the noninteracting model. (c) GMR comparison between gRISB (dark), RISB (medium) and HF (light).

In the case of a static electric field in the [110] direction the spin current $\mathbf{j}_s$ is orthogonal to the charge current $\mathbf{j}_c$ [5,33], hence we can use the Drude weight defined as

$$D^s_{ab} = \left\langle \frac{1}{V_{BZ}} \sum_{\mathbf{k}} \partial_{k_a} \partial_{k_b} H^s_{\mathbf{k}} \right\rangle - \Lambda^s_{ab}(\omega = 0) \tag{6}$$

to compute the charge-spin conversion ratio R as

$$R = \frac{|\mathbf{j}_s|}{|\mathbf{j}_c|} = \frac{\sqrt{\sum_a (j^{\uparrow}_a - j^{\downarrow}_a)^2}}{\sqrt{\sum_a (j^{\uparrow}_a + j^{\downarrow}_a)^2}} \tag{7}$$

where $j^s_a = \sum_\beta D^s_{ab} A_b$ and $A_b = A$ is the vector potential for $a, b = x, y$ directions.

We plot the ratio R in Fig. 3(b) with a positive sign for spin current in the $[-110]$ direction and negative for the opposite one. We notice an enhancement of R when increasing both doping and/or the interaction U/t. The ratio rises up to $R \approx 9\%$ for a typical value of $U/t = 20$, corresponding to an angle between the spin-up and spin-down currents of $\theta \approx 10^\circ$. We also notice that the spin current changes sign along a straight line in our U-δ diagram.

The inversion of the spin current is related to the different spin polarization of the carriers in x and y orbitals. The Drude weight in the x direction (D_{xx}) is dominated by the contribution of the electrons at the X point in the Brillouin zone (see the SM [63]). In this point the x orbital hosts a majority of spin-up carriers while the y orbital a majority of spin-down carriers. Tuning the doping or the interaction changes the density of the carriers around the X point differently from the two orbitals. As a consequence at a finite value of the doping δ or interaction U the spin-down and spin-up Drude weights cross allowing for an inversion of the spin currents. This phenomenon opens the possibility of changing the sign of the spin current tuning the interaction via mechanical or chemical pressure.

In order to assess how relevant strong correlations are to this altermagnetic ordering, we plot the band structure for an interaction $U/t = 20$ and doping $\delta = -0.15$ for Hartree-Fock (HF, left), RISB (center), and gRISB (right) in Fig. 3(a). The HF and RISB result are qualitatively similar, with the latter showing a moderate renormalization owing to the local Hubbard interaction. The gRISB band structure instead shows a stronger renormalization and a large transfer of spectral weight toward the lower and upper Hubbard bands. Moreover, the effect of strong correlation clearly reduces the nonrelativistic spin splitting and, more importantly, also changes the topology of the Fermi surface as shown in the insets of Fig. 3(a) with only gRISB predicting the presence of pockets around X and Y points in the Brillouin zone at large U/t. The presence of Dirac band crossing along the ΓX, ΓY, MX, and MY lines is present only in the gRISB calculations for strong interactions. The reason is the existence of the following critical condition on the intra-orbital magnetic gap (Δ_{mag}) above which the Dirac points disappear (see the SM [63] and [20]),

$$\frac{\Delta_{\text{mag}}}{|t_1 - t_2|} \leqslant 1. \tag{8}$$

The reduction of the magnetic gap in gRISB is a key ingredient for the persistence of Dirac points. As shown in Fig. 3(c), the giant magnetoresistance, defined as

$$GMR = \frac{1}{2}\left(\frac{\sigma^{\uparrow}_{xx}}{\sigma^{\downarrow}_{xx}} + \frac{\sigma^{\downarrow}_{xx}}{\sigma^{\uparrow}_{xx}} - 2 \right) \tag{9}$$

is also dramatically reduced by the inclusion of the high-energy ghosts improving the description of dynamical correlation effects. We observe indeed a reduction of a factor of almost 5 when comparing gRISB to RISB in the large interaction limit. This effect could partially resolve the mismatch between density functional theory predictions of ALM and the lack of spin-gap resolution in ARPES experiments.

Conclusions and outlook. We proposed a microscopic mechanism for interaction-generated altermagnetism linked to itinerant magnetism in the vicinity of a simple van Hove singularity, and we reported numerical evidence for its realization in a two-orbital model whose noninteracting band structure was introduced to describe iron-based superconductors. The altermagnetic state appears in a wide range of dopings and values of the interaction strength, presenting a maximum of the order parameter centered near the van Hove singularity δ_{vH}.

We analyzed the charge-spin conversion ratio responsible for the spin-splitter effect of the altermagnetic state and we observed a change of the spin current direction as a function of doping and interaction. This phenomenon opens the intriguing possibility to control the direction of the spin-current tuning the interaction exerting mechanical or chemical pressure on candidate materials.

Finally, we discussed the effect of strong correlations beyond mean-field in the theoretical description. These clearly affect the nature of the altermagnetic state changing the shape of the band structure and the topology of the Fermi surface. As a result, they reduce the altermagnetic spin gap and giant magnetoresistance with respect to simple mean-field calculations (Hartree-Fock). This effect could justify the difficulties to experimentally find photoemission evidence for altermagnetism in strongly correlated compounds. We note that a mechanism related to van Hove singularities has been proposed for κ-Cl in Ref. [21], which, unlike here, requires two coincident van Hove singularities at the M point to stabilize altermagnetic ordering.

Possible realizations of this mechanism could be found in Fe-based materials where evidence for altermagnetism has been reported for hematite ($\alpha - Fe_2O_3$) [19] and FeSe [18]. Further, systems where the t2g orbital physics is dominant, like Ca_2RuO_4 [8], could be suitable platform when the t2g bands are partially filled. Another promising platform are moiré systems, where electronic properties can be tailored precisely and a wide palette of systems can be designed. In this context, evidence of itinerant ferromagnetism linked to the presence of a van Hove singularity [66–68] and numerical evidence of altermagnetic ordering [69,70] have been reported.

In general, we emphasize the three key ingredients of our mechanism: (i) Two anisotropic orbitals related by a proper or improper rotation (e.g., in the model we present the x and y orbitals are related by C_{4z} symmetry), (ii) a strong

local Hubbard interaction U and hoppings between the two orbitals to generate direct interorbital spin exchange, and (iii) the presence of a vHs at an incommensurate filling promoting itinerant magnetic properties.

Moreover, frustration caused by the lattice (e.g., triangular lattice) or caused by hopping terms beyond nearest-neighbors (e.g., t_3 in this paper) opposes to bipartite ordering, hence favoring our altermagnetic state. In addition, materials with the previous properties and an inverted Hund's coupling J arising from electron-lattice coupling [71,72] may have an increased tendency to anti-align the spins on different orbitals, assisting the altermagnetic ordering we presented. Conversely, a positive sign J would only favor interorbital spin alignment. While for some materials, such as Ca_2RuO_4 [8], it is reasonable to expect that our altermagnetic order will survive, beyond a certain value of J the energetic gap between the spin-aligned and anti-aligned phases (see SM [63]) should lead to its disappearance.

In this paper, we have not considered the effect of spin-orbit coupling. We do not expect this to spoil our mechanism [5], but rather to enrich the phase diagram by breaking spin collinearity, thereby giving rise to nontrivial band topology [22,73].

Acknowledgments. We are grateful to C. Autieri, G. Bellomia, M. Fabrizio, R. Fernandes, M. Ferraretto, E. Linnér, J. Skolimowski, and A. Toschi for helpful discussions. This work has been supported by PNRR MUR Projects No. CN00000013-ICSC and No. PE0000023-NQSTI and by MUR via PRIN 2020 (Prot. 2020JLZ52N 002) programs, PRIN 2022 (Prot. 20228YCYY7).

[1] L. Šmejkal, J. Sinova, and T. Jungwirth, Beyond conventional ferromagnetism and antiferromagnetism: A phase with nonrelativistic spin and crystal rotation symmetry, Phys. Rev. X **12**, 031042 (2022).

[2] L. Šmejkal, J. Sinova, and T. Jungwirth, Emerging research landscape of altermagnetism, Phys. Rev. X **12**, 040501 (2022).

[3] D.-F. Shao, S.-H. Zhang, M. Li, C. B. Eom, and E. Y. Tsymbal, Spin-neutral currents for spintronics, Nat. Commun. **12**, 7061 (2021).

[4] H. Bai, L. Han, X. Y. Feng, Y. J. Zhou, R. X. Su, Q. Wang, L. Y. Liao, W. X. Zhu, X. Z. Chen, F. Pan, X. L. Fan, and C. Song, Observation of spin splitting torque in a collinear antiferromagnet RuO_2, Phys. Rev. Lett. **128**, 197202 (2022).

[5] R. González-Hernández, L. Šmejkal, K. Výborný, Y. Yahagi, J. Sinova, T. Jungwirth, and J. Železný, Efficient electrical spin splitter based on nonrelativistic collinear antiferromagnetism, Phys. Rev. Lett. **126**, 127701 (2021).

[6] R. M. Sattigeri, G. Cuono, and C. Autieri, Altermagnetic surface states: Towards the observation and utilization of altermagnetism in thin films, interfaces and topological materials, Nanoscale **15**, 16998 (2023).

[7] A. Fakhredine, R. M. Sattigeri, G. Cuono, and C. Autieri, Interplay between altermagnetism and nonsymmorphic symmetries generating large anomalous Hall conductivity by semi-Dirac points induced anticrossings, Phys. Rev. B **108**, 115138 (2023).

[8] G. Cuono, R. M. Sattigeri, J. Skolimowski, and C. Autieri, Orbital-selective altermagnetism and correlation-enhanced spin-splitting in strongly-correlated transition metal oxides, J. Magn. Magn. Mater. **586**, 171163 (2023).

[9] M. J. Grzybowski, C. Autieri, J. Domagala, C. Krasucki, A. Kaleta, S. Kret, K. Gas, M. Sawicki, R. Bożek, J. Suffczyński, and W. Pacuski, Wurtzite vs. Rock-salt MnSe epitaxy: Electronic and altermagnetic properties, Nanoscale **16**, 6259 (2024).

[10] F. Ferrari and R. Valenti, Altermagnetism on the Shastry-Sutherland lattice, Phys. Rev. B **110**, 205140 (2024).

[11] R. B. Regmi, H. Bhandari, B. Thapa, Y. Hao, N. Sharma, J. McKenzie, X. Chen, A. Nayak, M. E. Gazzah, B. G. Márkus *et al.*, Altermagnetism in the layered intercalated transition metal dichalcogenide $CoNb_4Se_8$, arXiv:2408.08835.

[12] J. W. González, A. M. León, C. González-Fuentes, and R. A. Gallardo, Altermagnetism in two dimensional Ca-Ru-O perovskite, arXiv:2408.08999.

[13] P.-H. Chang and I. I. Mazin, The mysterious magnetic ground state of Ba14MnBi11 is likely altermagnetic, arXiv:2407.16019.

[14] O. E. Parfenov, D. V. Averyanov, I. S. Sokolov, A. N. Mihalyuk, O. A. Kondratev, A. N. Taldenkov, A. M. Tokmachev, and V. G. Storchak, Pushing an altermagnet to the ultimate 2D limit: Evidence of symmetry breaking in monolayers of GdAlSi, arXiv:2406.07172.

[15] A. Hariki, T. Okauchi, Y. Takahashi, and J. Kuneš, Determination of the Néel vector in rutile altermagnets through x-ray magnetic circular dichroism: The case of MnF_2, Phys. Rev. B **110**, L100402 (2024).

[16] A. Hariki, A. Dal Din, O. J. Amin, T. Yamaguchi, A. Badura, D. Kriegner, K. W. Edmonds, R. P. Campion, P. Wadley, D. Backes, L. S. I. Veiga, S. S. Dhesi, G. Springholz, L. Šmejkal, K. Výborný, T. Jungwirth, and J. Kuneš, X-ray magnetic circular dichroism in altermagnetic α-MnTe, Phys. Rev. Lett. **132**, 176701 (2024).

[17] M. Milivojević, M. Orozović, S. Picozzi, M. Gmitra, and S. Stavrić, Interplay of altermagnetism and weak ferromagnetism in two-dimensional RuF_4, 2D Mater. **11**, 035025 (2024).

[18] I. Mazin, R. González-Hernández, and L. Šmejkal, Induced monolayer altermagnetism in $MnP(S,Se)_3$ and FeSe, arXiv:2309.02355.

[19] E. F. Galindez-Ruales, L. Šmejkal, S. Das, E. Baek, C. Schmitt, F. Fuhrmann, A. Ross, R. González-Hernández, A. Rothschild, J. Sinova, C. Y. You, G. Jakob, and M. Kläui, Altermagnetism in the hopping regime, arXiv:2310.16907.

[20] L. D. Re, Dirac points and topological phases in correlated altermagnets, arXiv:2408.14288.

[21] Y. Yu, H.-G. Suh, M. Roig, and D. F. Agterberg, Altermagnetism from coincident van Hove singularities: Application to κ-Cl, arXiv:2402.05180.

[22] D. S. Antonenko, R. M. Fernandes, and J. W. F. Venderbos, Mirror Chern bands and Weyl nodal loops in altermagnets, arXiv:2402.10201.

[23] H.-Y. Ma, M. Hu, N. Li, J. Liu, W. Yao, J.-F. Jia, and J. Liu, Multifunctional antiferromagnetic materials with giant piezomagnetism and noncollinear spin current, Nat. Commun. **12**, 2846 (2021).

[24] M. Hu, X. Cheng, Z. Huang, and J. Liu, Catalogue of *c*-paired spin-valley locking in antiferromagnetic systems, arXiv:2407.02319.

[25] M. Roig, A. Kreisel, Y. Yu, B. M. Andersen, and D. F. Agterberg, Minimal models for altermagnetism, Phys. Rev. B **110**, 144412 (2024).

[26] S. G. Jeong, I. H. Choi, S. Nair, L. Buiarelli, B. Pourbahari, J. Y. Oh, N. Bassim, A. Seo, W. S. Choi, R. M. Fernandes, T. Birol, L. Zhao, J. S. Lee, and B. Jalan, Altermagnetic polar metallic phase in ultra-thin epitaxially-strained RuO2 films, arXiv:2405.05838.

[27] Z. Lin, D. Chen, W. Lu, X. Liang, S. Feng, K. Yamagami, J. Osiecki, M. Leandersson, B. Thiagarajan, J. Liu, C. Felser, and J. Ma, Observation of giant spin splitting and *d*-wave spin texture in room temperature altermagnet RuO_2, arXiv:2402.04995.

[28] P. Keßler, L. Garcia-Gassull, A. Suter, T. Prokscha, Z. Salman, D. Khalyavin, P. Manuel, F. Orlandi, I. I. Mazin, R. Valentı, and S. Moser, Absence of magnetic order in RuO_2: Insights from μSR spectroscopy and neutron diffraction, arXiv:2405.10820.

[29] B. Jiang, M. Hu, J. Bai, Z. Song, C. Mu, G. Qu, W. Li, W. Zhu, H. Pi, Z. Wei *et al.*, Discovery of a metallic room-temperature d-wave altermagnet Kv2Se2O, arXiv:2408.00320.

[30] F. Zhang, X. Cheng, Z. Yin, C. Liu, L. Deng, Y. Qiao, Z. Shi, S. Zhang, J. Lin, Z. Liu *et al.*, Crystal-symmetry-paired spin-valley locking in a layered room-temperature antiferromagnet, arXiv:2407.19555.

[31] T. Osumi, S. Souma, T. Aoyama, K. Yamauchi, A. Honma, K. Nakayama, T. Takahashi, K. Ohgushi and T. Sato, Observation of a giant band splitting in altermagnetic MnTe, Phys. Rev. B **109**, 115102 (2024).

[32] S. Reimers, L. Odenbreit, L. Šmejkal, V. N. Strocov, P. Constantinou, A. B. Hellenes, R. Jaeschke Ubiergo, W. H. Campos, V. K. Bharadwaj, A. Chakraborty *et al.*, Direct observation of altermagnetic band splitting in CrSb thin films, Nat. Commun. **15**, 2116 (2024).

[33] V. Leeb, A. Mook, L. Šmejkal, and J. Knolle, Spontaneous formation of altermagnetism from orbital ordering, Phys. Rev. Lett. **132**, 236701 (2024).

[34] T. Sato, S. Haddad, I. C. Fulga, F. F. Assaad, and J. van den Brink, Altermagnetic anomalous Hall effect emerging from electronic correlations, Phys. Rev. Lett. **133**, 086503 (2024).

[35] A. Bose, S. Vadnais, and A. Paramekanti, Altermagnetism and superconductivity in a multiorbital t-*J* model, arXiv:2403.17050.

[36] P. Das, V. Leeb, J. Knolle, and M. Knap, Realizing altermagnetism in Fermi-Hubbard models with ultracold atoms, Phys. Rev. Lett. **132**, 263402 (2024).

[37] N. Heinsdorf, Altermagnetic instabilities from quantum geometry, arXiv:2410.12789.

[38] Y. Nagaoka, Ferromagnetism in a narrow, almost half-filled *s* band, Phys. Rev. **147**, 392 (1966).

[39] J. E. Hirsch, Two-dimensional Hubbard model: Numerical simulation study, Phys. Rev. B **31**, 4403 (1985).

[40] H. Q. Lin and J. E. Hirsch, Two-dimensional Hubbard model with nearest- and next-nearest-neighbor hopping, Phys. Rev. B **35**, 3359 (1987).

[41] S. Raghu, X.-L. Qi, C.-X. Liu, D. J. Scalapino, and S.-C. Zhang, Minimal two-band model of the superconducting iron oxypnictides, Phys. Rev. B **77**, 220503(R) (2008).

[42] M. Ulmke, Ferromagnetism in the Hubbard model on fcc-type lattices, Eur. Phys. J. B **1**, 301 (1998).

[43] I. Morera, M. Kanász-Nagy, T. Smolenski, L. Ciorciaro, A. Imamoğlu, and E. Demler, High-temperature kinetic magnetism in triangular lattices, Phys. Rev. Res. **5**, L022048 (2023).

[44] M. Lebrat, M. Xu, L. H. Kendrick, A. Kale, Y. Gang, P. Seetharaman, I. Morera, E. Khatami, E. Demler, and M. Greiner, Observation of Nagaoka polarons in a Fermi–Hubbard quantum simulator, Nature (London) **629**, 317 (2024).

[45] M. Xu, L. H. Kendrick, A. Kale, Y. Gang, G. Ji, R. T. Scalettar, M. Lebrat, and M. Greiner, Frustration-and doping-induced magnetism in a Fermi–Hubbard simulator, Nature (London) **620**, 971 (2023).

[46] R. Hlubina, S. Sorella, and F. Guinea, Ferromagnetism in the two dimensional $t - t'$ Hubbard model at the van Hove density, Phys. Rev. Lett. **78**, 1343 (1997).

[47] D. V. Chichinadze, L. Classen, and A. V. Chubukov, Valley magnetism, nematicity, and density wave orders in twisted bilayer graphene, Phys. Rev. B **102**, 125120 (2020).

[48] L. Classen, A. V. Chubukov, C. Honerkamp, and M. M. Scherer, Competing orders at higher-order van Hove points, Phys. Rev. B **102**, 125141 (2020).

[49] N. Lanatà, Operatorial formulation of the ghost rotationally invariant slave-boson theory, Phys. Rev. B **105**, 045111 (2022).

[50] F. Lechermann, A. Georges, G. Kotliar, and O. Parcollet, Rotationally invariant slave-boson formalism and momentum dependence of the quasiparticle weight, Phys. Rev. B **76**, 155102 (2007).

[51] A. Isidori and M. Capone, Rotationally invariant slave bosons for strongly correlated superconductors, Phys. Rev. B **80**, 115120 (2009).

[52] N. Lanatà, T.-H. Lee, Y.-X. Yao, and V. Dobrosavljević, Emergent Bloch excitations in Mott matter, Phys. Rev. B **96**, 195126 (2017).

[53] D. Guerci, M. Capone, and M. Fabrizio, Exciton Mott transition revisited, Phys. Rev. Mater. **3**, 054605 (2019).

[54] M. S. Frank, T.-H. Lee, G. Bhattacharyya, P. K. H. Tsang, V. L. Quito, V. Dobrosavljević, O. Christiansen, and N. Lanatà, Quantum embedding description of the Anderson lattice model with the ghost Gutzwiller approximation, Phys. Rev. B **104**, L081103 (2021).

[55] C. Mejuto-Zaera and M. Fabrizio, Efficient computational screening of strongly correlated materials: Multiorbital phenomenology within the ghost Gutzwiller approximation, Phys. Rev. B **107**, 235150 (2023).

[56] D. Guerci, M. Capone, and N. Lanatà, Time-dependent ghost Gutzwiller nonequilibrium dynamics, Phys. Rev. Res. **5**, L032023 (2023).

[57] T.-H. Lee, C. Melnick, R. Adler, N. Lanatà, and G. Kotliar, Accuracy of ghost-rotationally-invariant slave-boson theory for multiorbital Hubbard models and realistic materials, Phys. Rev. B **108**, 245147 (2023).

[58] T.-H. Lee, N. Lanatà, and G. Kotliar, Accuracy of ghost rotationally invariant slave-boson and dynamical mean field theory as a function of the impurity-model bath size, Phys. Rev. B **107**, L121104 (2023).

[59] C. Mejuto-Zaera, Quantum embedding for molecules using auxiliary particles—the ghost Gutzwiller ansatz, Faraday Discuss. **254**, 653 (2024).

[60] T.-H. Lee, C. Melnick, R. Adler, X. Sun, Y. Yao, N. Lanatà, and G. Kotliar, Charge self-consistent density functional theory plus ghost rotationally invariant slave-boson theory for correlated materials, Phys. Rev. B **110**, 115126 (2024).

[61] M. Fabrizio, Gutzwiller description of non-magnetic Mott insulators: Dimer lattice model, Phys. Rev. B **76**, 165110 (2007).

[62] N. Lanatà, Y. Yao, C.-Z. Wang, K.-M. Ho, and G. Kotliar, Phase diagram and electronic structure of praseodymium and plutonium, Phys. Rev. X **5**, 011008 (2015).

[63] See Supplemental Material at http://link.aps.org/supplemental/10.1103/PhysRevB.111.L020401 for a summary of the computation of the conductivity in linear response, a complement to the discussion on the tuneability of the spin currents in the strong coupling altermagnetic phase, and a brief recap of the main equations in the gRISB formalism.

[64] B. S. Shastry and B. Sutherland, Twisted boundary conditions and effective mass in Heisenberg-Ising and Hubbard rings, Phys. Rev. Lett. **65**, 243 (1990).

[65] D. J. Scalapino, S. R. White, and S. C. Zhang, Superfluid density and the Drude weight of the Hubbard model, Phys. Rev. Lett. **68**, 2830 (1992).

[66] Y. Tang, L. Li, T. Li, Y. Xu, S. Liu, K. Barmak, K. Watanabe, T. Taniguchi, A. H. Macdonald, J. Shan, and K. F. Mak, Simulation of Hubbard model physics in WSe_2/WS_2 moiré superlattices, Nature (London) **579**, 353 (2020).

[67] K. Lee, P. Sharma, O. Vafek, and H. J. Changlani, Triangular lattice Hubbard model physics at intermediate temperatures, Phys. Rev. B **107**, 235105 (2023).

[68] P. Potasz, N. Morales-Durán, N. C. Hu, and A. H. MacDonald, Itinerant ferromagnetism in transition metal dichalcogenide moiré superlattices, Phys. Rev. B **109**, 045144 (2024).

[69] S. Sheoran and S. Bhattacharya, Nonrelativistic spin splittings and altermagnetism in twisted bilayers of centrosymmetric antiferromagnets, Phys. Rev. Mater. **8**, L051401 (2024).

[70] S.-D. Guo, Y. Liu, and C.-C. Liu, Valley polarization in twisted altermagnetism, arXiv:2406.13950.

[71] M. Capone, M. Fabrizio, C. Castellani, and E. Tosatti, Strongly correlated superconductivity, Science **296**, 2364 (2002).

[72] M. Capone, M. Fabrizio, C. Castellani, and E. Tosatti, Colloquium: Modeling the unconventional superconducting properties of expanded A_3C_{60} fullerides, Rev. Mod. Phys. **81**, 943 (2009).

[73] L. Šmejkal, R. González-Hernández, T. Jungwirth, and J. Sinova, Crystal time-reversal symmetry breaking and spontaneous Hall effect in collinear antiferromagnets, Sci. Adv. **6**, eaaz8809 (2020).